Compendium of NASA Goddard Space Flight Center's Recent Radiation Effects Test Results

Martha V. O'Bryan, Seth S. Roffe, Edward P. Wilcox, Michael J. Campola, Jason M. Osheroff, Megan C. Casey, Matthew B. Joplin, Thomas A. Carstens, Jonathan D. Barth, Landen D. Ryder, Kaitlyn, L. Ryder, Jean-Marie Lauenstein, Adia M. Wood, and Peter J. Majewicz

Abstract-- We present results and analysis investigating the effects of radiation on a variety of candidate spacecraft electronics to heavy ion and proton induced single-event effects (SEE), proton-induced displacement damage dose (DDD), and total ionizing dose (TID).

***Index Terms* — Single event effects, space radiation reliability, spacecraft electronics.**

I. INTRODUCTION

NASA spacecraft are subjected to a harsh space environment that includes exposure to various types of radiation. The performance of electronic devices in a space radiation environment is often limited by their susceptibility to single-event effects (SEE), total ionizing dose (TID), and displacement damage dose (DDD). Ground-based testing is used to evaluate candidate spacecraft electronics to determine risk to spaceflight applications. Interpreting the results of radiation testing of complex devices is quite difficult. Given the rapidly changing nature of technology, radiation test data are most often application-specific and adequate understanding of the test conditions is critical [1].

Studies discussed herein were undertaken to establish the application-specific sensitivities of candidate spacecraft and emerging electronic devices to single-event SEE including single-event upset (SEU), single-event latchup (SEL), single-event gate rupture (SEGR), single-event burnout (SEB), single-event transient (SET), TID, enhanced low dose rate sensitivity (ELDRS), and DDD effects. All tests were performed between February 2023 and February 2024.

This work was supported in part by the NASA Electronic Part and Packaging Program (NEPP) and NASA Flight Projects.

Martha V. O'Bryan is with Science Systems and Applications (SSAI), Inc., Lanham, MD, 20706 (USA) work performed for NASA Goddard Space Flight Center, phone: 301-286-1412, email: martha.v.obryan@nasa.gov.

Seth S. Roffe, Edward P. Wilcox, Michael J. Campola, Jason M. Osheroff, Megan C. Casey, Matthew B. Joplin, Thomas A. Carstens, Jonathan D. Barth, Landen D. Ryder, Kaitlyn, L. Ryder, Jean-Marie Lauenstein, Adia M. Wood, and Peter J. Majewicz are with NASA/GSFC, 61, Greenbelt, MD 20771 (USA), Seth S. Roffe, phone: 301-286-7721, email: seth.roffe@nasa.gov or Edward P. Wilcox, phone: 301-286-5427, email: ted.wilcox@nasa.gov.

II. TEST TECHNIQUES AND SETUP

A. Test Method

Unless otherwise noted, SEE testing was performed in accordance with JESD57A test procedures [2]. Depending on the Device Under Test (DUT) and the test objectives, one or two SEE test methods were typically used:

a) *Dynamic* – The DUT was exercised and monitored continuously while being irradiated. The type of input stimulus and output data capture methods are highly device- and application-dependent. In all cases the power supply levels were actively monitored during irradiation. These results are highly application-dependent and may only represent the specific operational mode tested.

b) *Static/Biased* – The DUT was provided basic power and configuration information (where applicable), but not actively operated during irradiation. The device output may or may not have been actively monitored during irradiation, while the power supply current was actively monitored for changes.

In SEE experiments, DUTs were monitored for soft errors, such as SEUs, and for hard errors, such as SELs. Detailed descriptions of the types of errors observed are noted in the individual test reports.

SET testing was performed using high-speed oscilloscopes controlled via National Instruments LabVIEW® [3]. Individual criteria for SETs are specific to the device and application being tested. Please see the individual test reports for details [4, 5].

Heavy ion SEE sensitivity experiments include measurement of the linear energy transfer threshold (LET_{th}) and cross section at the maximum measured LET. The LET_{th} is defined as the maximum LET value at which no effect was observed at an effective fluence of 1×10^7 particles/cm^2. In the case where events are observed at the smallest LET tested, LET_{th} will either be reported as less than the lowest measured LET or determined approximately as the LET_{th} parameter from a Weibull fit.

TID testing was performed using MIL-STD-883, Test Method 1019.9 [6] unless otherwise noted as research. All tests were performed at room temperature and with nominal power supply voltages, unless otherwise noted. Based on the application, samples would be tested in a biased and/or unbiased configuration. Functionality and parametric changes were measured after step irradiations (for example: every 10 krad(Si)).

B. Test Facilities – SEE

Heavy ion experiments were conducted at the Texas A&M University Cyclotron (TAMU) [7], Lawrence Berkeley National Laboratory (LBNL) 88-inch cyclotron [8], Michigan State University's Facility for Rare Isotope Beams (FRIB) [9], and Brookhaven National Laboratory's NASA Space Radiation Laboratory (NSRL) [10]. These facilities provide a variety of ions over a range of energies for testing.

C. Test Facilities – TID

TID testing was performed using a gamma source [11]. Dose rates used for testing were between 10 mrad(Si)/s and ~50 krad(Si)/s.

D. Test Facilities – DDD

Proton DDD tests were performed at the University of California at Davis Crocker Nuclear Laboratory (UCD - CNL) [12] using a 76" cyclotron and energy of 64 MeV, and at Massachusetts General Hospital (MGH) Francis H. Burr Proton Therapy [13].

III. TEST RESULTS OVERVIEW

Principal investigators are listed in Table I. Abbreviations and conventions are listed in Table II. SEE results are summarized in Table III. TID and DDD results are summarized in Table IV. All parts tested between February 2023 and February 2024. Unless otherwise noted all LETs are in MeV•cm^2/mg and all cross sections are in cm^2/device. All SEL tests are performed to a fluence of 1×10^7 particles/cm^2 unless otherwise noted. Proton tests were performed at a flux of $1x10^7$ to $1x10^9$ p+/cm^2-s. The fluence was to until an event was observed, or $1x10^{10}$ to $1x10^{11}$ p+/cm^2 at a given energy (i.e. 200 MeV, etc).

TABLE I: LIST OF PRINCIPAL INVESTIGATORS

Principal Investigator (PI)	Abbreviation
Megan C. Casey	MCC
Matthew B. Joplin	MBJ
Jean-Marie Lauenstein	JML
Jason M. Osheroff	JMO
Seth Roffe	SR
Kaitlyn L. Ryder	KLR
Landen D. Ryder	LR
Edward (Ted) Wilcox	TW

TABLE II: ACRONYM LIST

Acronym	Definition
σ	cross section (cm^2/device, unless specified as cm^2/bit)
σ_{maxm}	cross section at maximum measured LET (cm^2/device, unless specified as cm^2/bit)
<	SEE observed at lowest tested LET
>	no SEE observed at highest tested LET
CMOS	Complementary Metal Oxide Semiconductor
DDD	Displacement Damage Dose
DDR3	Double Data Rate 3
DDR4	Double Data Rate 4
DUT	Device Under Test
FPGA	Field Programmable Gate Array
FRIB	Michigan State University's Facility for Rare Isotope Beams
GPU	Graphic Processing Unit
GSFC	Goddard Space Flight Center
LBNL	Lawrence Berkeley National Laboratory
LCD	Liquid-Crystal Display
LDC	Lot Date Code
LED	Light Emitting Diode
LET	Linear Energy Transfer
LETth	Linear Energy Transfer threshold (the maximum LET value at which no effect was observed at an effective fluence of $1x10^7$ particles/cm^2 - in MeV•cm^2/mg
LPDDR	Low Power Double Data Rate
MFTF	mean fluence to failure
MGH FRIB	Massachusetts General Hospital (MGH) Francis H. Burr Proton Therapy, Facility for Rare Isotope Beams (FRIB)
MSU	Michigan State University
NEPP	NASA Electronics Parts and Packaging
NOR	Non-volatile storage technology optimized for random access capabilities
NSRL	Brookhaven National Laboratory's NASA Space Radiation Laboratory
n/a	Not Available
PI	Principal Investigator
REAG	Radiation Effects & Analysis Group
ROIC	Readout-Integrated Circuit
SCA	Sensor Chip Assembly
SEB	Single-Event Burnout
SEE	Single-Event Effect
SEFI	Single-Event Functional Interrupt
SEGR	Single-Event Gate Rupture
SEL	Single-Event Latchup
SET	Single-Event Transient
SEU	Single-Event Upset
SSD	Solid State Drive
TAMU	Texas A&M University
TID	Total Ionizing Dose
UCD	University of California at Davis Crocker Nuclear Laboratory
V_{DS}	Drain-Source Voltage
V_{GS}	Gate-Source Voltage

TABLE III: SUMMARY OF SEE TEST RESULTS

Part Number	Manufacturer	LDC (REAG ID#)	Device Function	Technology	PI	Sample Size	Supply Voltage	Test Env.	Test Facility (Test Date)	Test Results: σ in cm²/device, unless otherwise specified
Memories										
MTFDHBK256TDP-1AT12AIYY	Micron	n/a (23-009)	NVMe Solid State Drive	NAND Flash	TW	7	3.3 V	Proton	MGH (Jan 2024)	Unrecoverable failures observed with 200 MeV protons only under active read-write testing. MFTF: $2.22 \times 10^{10}/cm^2$. Recoverable failures with power cycling observed with 200 MeV protons. MFTF: $1.56 \times 10^{9}/cm^2$ [14-15]
SDBPTPZ-085G-XI	Western Digital	n/a (23-010)	NVMe Solid State Drive	NAND Flash	TW	7	3.3 V	Proton	MGH (Jan 2024)	Unrecoverable failures (MFTF: $1.43 \times 10^{10}/cm^2$) observed with 200 MeV protons only under active read-write testing. Recoverable failures (MFTF: $1.86 \times 10^{10}/cm^2$) observed with 200 MeV protons during both reading and writing operations.
MT25QU512ABB	Micron	2YA15 (23-025)	Flash Memory	NOR	TW	5	1.8 - 2.0 V	Heavy Ion	LBNL (Dec 2023)	29.4 < SEL LET_{th} < 45.3 $MeVcm^2/mg$ at 55°C SEL LET_{th} < 29.4 at 82°C σ_{maxm} $9.09 \times 10^{-8} cm^2$ at 29.4 $MeVcm^2/mg$, 82°C SEU LET_{th} < 8.2 $MeVcm^2/mg$ SEU σ 1.8×10^{-16} cm^2/bit at 8.2 $MeVcm^2/mg$
Processing										
ZYNQ XC7Z020-1CLG400C	Xilinx	n/a (20-004)	FPGA and ARM Processor on TUL PYNQ-Z2 Board	CMOS	SR	1	12 V	Protons	MGH (Aug 2023)	Performing math operations increases reliability by the cross section metric when L2 cache is enabled by allowing critical cache to be flushed. L1 cache not large enough to store as much critical information, so disabling L2 cache trivially increases reliability. [16]
SAKURA-I	EdgeCortix	n/a (24-001)	AI Coprocessor (PCIe card)	16 GB LPDDR4	SR	1	12 V	Proton	MGH (Jan 2024)	No destructive SEEs observed at 200 MeV protons with a flux reaching ~ 10^9 p/cm^2 s. Data errors were observed in the form of inference mispredictions and changes in the output confidence scores. [17]
Diodes										
STTH208UFY	STMicroelectronics	n/a (22-021)	Diode	Si	MCC	25	800 V	Heavy Ion	MSU FSEE (Apr 2023)	SEB LET_{th} > 50.5 $MeVcm^2/mg$ at V_R = 800 V
RS1KFSHMWG	Taiwan Semiconductor	n/a (22-022)	Diode	Si	MCC	25	800 V	Heavy Ion	MSU FSEE (Apr 2023)	SEB LET_{th} > 50.5 $MeVcm^2/mg$ at V_R = 800 V
HS1KFS	Taiwan Semiconductor	n/a (22-023)	Diode	Si	MCC	25	800 V	Heavy Ion	MSU FSEE (Apr 2023)	SEB LET_{th} > 50.5 $MeVcm^2/mg$ at V_R = 800 V
SFF6661	SSDI	2248 (23-003)	N-Channel Power MOSFET	Si	LR/ JMO	11	0V, -5V, -10V	Heavy Ion	MSU FSEE (Apr 2023)	Tested at LET of 50.5 MeV•cm^2/mg; No destructive SEEs observed at 65 V_{DS} & 0 V_{GS}; No destructive SEEs observed at 55 V_{DS} & -5 V_{GS}; 3 (1) pass/(fail) at 70 V_{DS} & 0 V_{GS}; 3 fails at 75 V_{DS} & 0 V_{GS}; 4 fails at 55 V_{DS} & -10 V_{GS} [18]

Part Number	Manufacturer	LDC (REAG ID#)	Device Function	Technology	PI	Sample Size	Supply Voltage	Test Env.	Test Facility (Test Date)	Test Results: σ in cm²/device, unless otherwise specified
Miscellaneous										
TLK2711-SP	Texas Instruments	1828A (23-026)	Transceiver	0.25 µm CMOS	MCC	5	2.5 V	Heavy Ion	LBNL (Aug 2023)	SEL LET_{th} > 75.6 $MeVcm^2/mg$ @75°C
SN54LVTH574-SP	Texas Instruments	2040A (23-027)	Logic	CMOS	MCC	15	3.3 V	Heavy Ion	LBNL (Aug 2023)	SEL LET_{th} > 75.6 $MeVcm^2/mg$ @75°C
SSD1351	Soloman Systech	1431 (22-045)	Organic LED Display Drive	CMOS	LR	2	5 V	Heavy Ion	LBNL (Jun 2023)	SEFI LET_{th} < 1.2 MeV•cm^2/mg
HXD8357D	Himax Technologies	2050 (22-047)	LCD Display Driver	CMOS	LR	2	5 V	Heavy Ion	LBNL (Jun 2023)	SEFI LET_{th} < ~16 MeV•cm^2/mg. Potential range issues due to packaging constraints.

TABLE VI: SUMMARY OF TID and DDD TEST RESULTS

Part Number	Manufacturer	LDC or Wafer# (REAG ID#)	Device Function	PI	Sample Size	Test Env.	Test Facility (Test Date)	Test Results (Effect, Dose Level/Energy, Results)
Power Devices								
2N6284	Microchip	P2132CDWR (23-006)	Power Transistor	KLR	6	Gamma	GSFC (Aug 2023)	No degradation observed up to 59.6 krad(Si)
2N5154	VPT	B2321 (23-022)	Power Transistor	KLR	6	Gamma	GSFC (Dec 2023)	No degradation observed up to 61 krad(Si)
Photonics								
EYP-RWL-0808-00800-4000-BFW09-0000	Toptica-Eagleyard	n/a (23-011)	808-nm Laser Diode	MBJ	2	Proton DDD	UCD (Aug 2023)	No observable degradation up to 63-MeV proton fluence of 5.6E11 p/cm^2.
EYP-RWL-0808-00800-4000-BFW09-0000	Toptica-Eagleyard	n/a (23-011)	808-nm Laser Diode	MBJ	2	Gamma	GSFC (Dec 2023)	No degradation observed up to 80 krad(Si).
IF-HS1	Coherent-Dilas	n/a (23-012)	976-nm Laser Diode	MBJ	2	Proton DDD	UCD (Aug 2023)	No observable degradation up to 63-MeV proton fluence of 5.52E11 p/cm^2.
IF-HS1	Coherent-Dilas	n/a (23-012)	976-nm Laser Diode	MBJ	2	Gamma	GSFC (Dec 2023)	No degradation observed up to 80 krad(Si).
CMDFB1030A	II-VI	n/a (23-013)	1030-nm Laser Diode	MBJ	1	Proton DDD	UCD (Aug 2023)	No observable degradation up to 63-MeV proton fluence of 5.87E11 p/cm^2.
CMDFB1030A	II-VI	n/a (23-013)	1030-nm Laser Diode	MBJ	1	Gamma	GSFC (Dec 2023)	No degradation observed up to 80 krad(Si).
EPM605	JDSU/Lumentum	n/a (23-014)	Photodiode	MBJ	2	Proton DDD	UCD (Aug 2023)	Photodiode degradation of dark current at 63-MeV proton fluence<7.5E10 p/cm^2.
EPM605	JDSU/Lumentum	n/a (23-014)	Photodiode	MBJ	2	Gamma	GSFC (Dec 2023)	No degradation observed up to 80 krad(Si).
C30665GH-LC	Excelitas	n/a (23-015)	Photodiode	MBJ	1	Proton DDD	UCD (Aug 2023)	Photodiode degradation of dark current and responsivity at 63-MeV proton fluence<7.5E10 p/cm^2.
C30665GH-LC	Excelitas	n/a (23-015)	Photodiode	MBJ	1	Gamma	GSFC (Dec 2023)	No degradation observed up to 80 krad(Si).
J22-5IR03M-1.7	Teledyne	n/a (23-016)	Photodiode	MBJ	1	Proton DDD	UCD (Aug 2023)	Photodiode degradation of dark current at 63-MeV proton fluence<7.5E10 p/cm^2.
J22-5IR03M-1.7	Teledyne	n/a (23-016)	Photodiode	MBJ	1	Gamma	GSFC (Dec 2023)	No degradation observed up to 80 krad(Si).
GAP3000	GPD	n/a (23-017)	Photodiode	MBJ	1	Proton DDD	UCD (Aug 2023)	Photodiode degradation of dark current at 63-MeV proton fluence <7.5E10 p/cm^2.
GAP3000	GPD	n/a (23-017)	Photodiode	MBJ	1	Gamma	GSFC (Dec 2023)	No degradation observed up to 80 krad(Si).
C30665GH	Excelitas	n/a (24-004)	Photodiode	MBJ	2	Proton DDD	UDC (Feb 2024)	Photodiode degradation of dark current at 63-MeV proton fluence<8.89E11 p/cm^2.
NIR-MPZ-LN-20	iXblue	n/a (23-018)	Optical Phase Modulator	MBJ	1	Proton DDD	UCD (Aug 2023)	No observable degradation up to a 63-MeV proton fluence of 5.89E11 p/cm^2.
NIR-MPZ-LN-20	iXblue	n/a (23-018)	Optical Phase Modulator	MBJ	1	Gamma	GSFC (Dec 2023)	No degradation observed up to 80 krad(Si).

Part Number	Manufacturer	LDC or Wafer# (REAG ID#)	Device Function	PI	Sample Size	Test Env.	Test Facility (Test Date)	Test Results (Effect, Dose Level/Energy, Results)
BBM2-NIR-MPX-LN-01	iXblue	n/a (23-019)	Optical Phase Modulator	MBJ	1	Proton DDD	UCD (Aug 2023)	No observable degradation up to a 63-MeV proton fluence of 5.89E11 p/cm^2.
BBM2-NIR-MPX-LN-01	iXblue	n/a (23-019)	Optical Phase Modulator	MBJ	1	Gamma	GSFC (Dec 2023)	No degradation observed up to 80 krad(Si).
SCD-T80156 rev A	DiCon	n/a (24-005)	Optical Switch	MBJ	2	Proton DDD	UCD (Feb 2024)	No observable degradation up to a 63-MeV proton fluence of 8.95E10 p/cm^2.
113-00148	Coherent Electro-Optics Technology	n/a (24-006)	High Power Isolator	MBJ	2	Proton DDD	UCD (Feb 2024)	No observable degradation up to a 63-MeV proton fluence of 8.95E10 p/cm^2.
OD-110L	Opti Diode	n/a (23-028)	GaAlAs 850 nm LED	JML	4	Proton DDD	UCD (Aug 2023)	Step irradiation to up to 63 MeV proton fluence of $3.40 \times 10^{12}/cm^2$ (451 krad(Si). Relative optical intensity decreased between 47.1% - 48.5% at the maximum dose; no spectral shift or widening of the output spectrum.[19]
NC4U334BR	Nichia	n/a (23-029)	AlGaN 280 nm LED	JML	2	Proton DDD	UCD (Aug 2023)	Step irradiation to up to 63 MeV proton fluence of $3.43 \times 10^{12}/cm^2$ (456 krad(Si). Relative optical intensity decreased ≤ 10% at max dose; no spectral shift or widening of output spectrum.
NCSU434C	Nichia	n/a (23-030)	AlGaN 280 nm LED	JML	2	Proton DDD	UCD (Aug 2023)	Step irradiation to up to 63 MeV proton fluence of $3.43 \times 10^{12}/cm^2$ (456 krad(Si). Relative optical intensity decreased ≤ 10% at max dose; no spectral shift or widening of output spectrum.
XFM-5050-UV	Luminus	n/a (23-031)	AlGaN 280 nm LED	JML	2	Proton DDD	UCD (Aug 2023)	Step irradiation to up to 63 MeV proton fluence of $3.43 \times 10^{12}/cm^2$ (456 krad(Si). Relative optical intensity decreased ≤ 10% at max dose; no spectral shift or widening of output spectrum.
Thermistors								
QT06020-142	Qti	n/a (23-020)	Thermistor	MBJ	2	Proton DDD	UCD (Aug 2023)	Thermistor showed variation in temperature linearity between 63-MeV-proton 7.5e10 p/cm^2 and 1.5e11 p/cm^2 fluence.
QT06020-142	Qti	n/a (23-020)	Thermistor	MBJ	2	Gamma	GSFC (Dec 2023)	No degradation observed up to 80 krad(Si).

IV. TEST RESULTS AND DISCUSSION

As in our past workshop compendia of GSFC test results, most devices under test have a detailed test report available online at http://radhome.gsfc.nasa.gov [4] and at http://nepp.nasa.gov [5] describing in further detail the test method, conditions, monitored parameters, and test results. This section contains a summary of testing performed on a selection of featured parts.

A. Micron MTFDHBK256TDP-1AT12AIYY SSD

An automotive-grade, small form factor solid-state drive (SSD) presents an interesting possibility for small satellite or advanced technology space missions if sufficient radiation tolerance can be demonstrated. The Micron MTFDHBK256TDP-1AT12AIYY is a 256 GB SSD built around 64-layer Intel-branded triple-level cell (TLC) NAND flash. As procured, it is an industrial-grade device from Micron's 2100AT/AI automotive/industrial product line.

1. Test Setup

Solid-state drives are complex systems with all the difficulties of any board-level radiation test. These devices were chemically decapsulated by NASA, revealing an internal PCIe controller chip, a four-die stack of flash, a low drop out (LDO) regulator, and numerous smaller components just within the single plastic-encapsulated ball-grid array device. Single-event effects testing at this level precludes detailed characterization of low-level device performance, including bit errors. Instead, the system itself is continuously operated in a manner that, ideally, reveals any radiation-induced failures as quickly as possible. As single fluence-to-failure measurements are difficult to apply to a space radiation environment, the test setup was automated to quickly gather a larger sample size during testing.

To both operate the part and autonomously attempt recovery from a radiation-induced event, while allowing broad-beam testing to access the entire board without decapsulation, a new test setup was developed. Numerous PCIe-to-USB adapters exist commercially, but all have their own active electronics in close proximity to (usually under) the SSD. To resolve this, an off-the-shelf PCIe extender module (below) centers the device under test (DUT) in the radiation beam while keeping active electronics 10cm or further from the beam, where they can be shielded if necessary. Furthermore, the gold fingers providing 3.3 V power from a host PC have been filed away and an external power connector added to power the SSD independently.

A PCIe-to-USB adapter, while sacrificing raw speed, still allows a data processing computer to connect with USB-C for 400 MB/s or faster data access in beam. The computer itself can be remotely controlled over Ethernet hundreds of feet away.

Test automation is provided by a National Instruments USB-6501 digital I/O module. The custom Python-based test code exercising the memory can command power supply interruptions and facility beam inhibits through this digital I/O module's connections to test hardware.

2. Operation During Test

To maintain realistic operating conditions, the devices were tested with 1 GB of pseudorandom data written and read from random locations (changing each cycle) through the SSD memory space. Each write/read loop takes about 10 seconds to complete at this scale. Operations were performed from a Windows 10-based computer using Python test code that used the wmic module to perform low level (raw) block operations.

Fig. 1 shows the DUT mounted to passive PCIe extender for testing. A complete, automated SEFI test looks as follows when viewed from the power supply logs (see Fig. 2).

Fig. 1. DUT mounted to passive PCIe extender for testing.

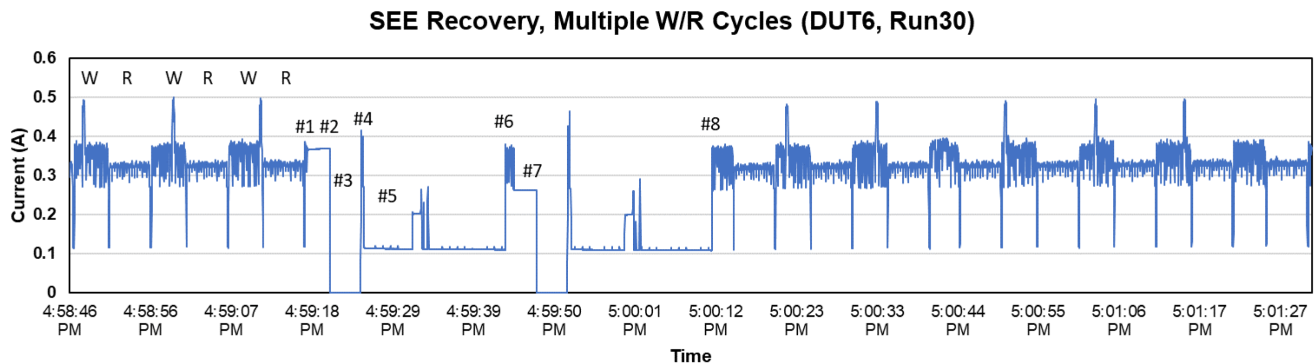

Fig. 2. Two SEFI observed and recovered in quick succession during 200 MeV proton testing.

In Fig. 2, the device performs three sets of write (W) and read (R) operations successfully, followed by an error event in the following write. The sequence below describes the subsequent events, marked with numbers on the chart in Fig. 2:

1. Initiation of a write command at 4:59:17 PM. The supply current elevates but is uncharacteristically flat.
2. Three seconds later at 4:59:20 PM the test software throws an exception when the write has failed to complete. This is classified as a timeout error.
3. The power supply is disabled for four seconds and the proton beam is inhibited.
4. At 4:59:24 PM power is restored
5. The device is allowed 20 seconds to initialize, still without beam applied.
6. At 4:59:44 PM the beam is uninhibited and testing (the incomplete write) resumes
7. Writing proceeds successfully for about 2 seconds until it again hangs for 3 seconds, triggering a timeout error and a repeat of the recovery in steps 3-6).
8. Writing resumes after the second recovery and completes. The subsequent read operation is successful, along with the depicted write and read cycles afterwards.

3. *Test Results*

The results of testing six devices at the Francis H. Burr Proton Therapy Center at Massachusetts General Hospital are summarized in Table I, presented as fluence-between-failure statistics, all with 200 MeV protons and under active reading and writing.

TABLE I. FLUENCE BETWEEN FAILURE WITH PROTON IRRADIATIONS

Device #	Total Failure Events	Total Biased Fluence	Mean Fluence Between Failure	Tested until unrecoverable error occurred?
Micron_2	2	4.28E+09	2.14E+09	Yes
Micron_3	7	6.97E+09	9.96E+08	Yes
Micron_4	4	8.82E+09	2.21E+09	Yes
Micron_5	14	1.46E+10	1.04E+09	Yes
Micron_6	13	2.06E+10	1.58E+09	No
Micron_7	9	2.38E+10	1.98E+09	No
Micron_8	9	1.26E+10	9.42E+08	No
sum	*58*	*9E+10*	*1.56E+09*	

Recoverable failures were those that were resolved immediately upon automated power supply cycling and allowed continued operation as normal. Unrecoverable failures did not recover with power supply cycling, even with manual intervention. The failure mechanism was consistent, that read operations were successful, but write operations would immediately fail. After testing, debugging attempts with these drives indicated that the controller firmware was reporting the drive to be in a possible write protect mode, but no further details are available at this time. [14-15]

B. *TUL PYNQ-Z2 Board with Xilinx ZYNQ XC7Z020-1CLG400C SoC*

The TUL PYNQ-Z2 was tested in August of 2023 under 200 MeV protons at Massachusetts General Hospital's Burr Proton Therapy Center, shown in Fig. 3. The PYNQ-Z2 employs a Zynq-7020 System-on-Chip (SoC) which contains an Artix-7 FPGA fabric and an ARM Cortex-A9 CPU. The operating system on the ARM Processing side was the primary target for this experiment. The purpose of this experiment was to understand how the operating system (OS) of a processor affects the target's reliability, in particular the cross section, where a failure was defined as a SEFI. Sixteen different Linux OS configurations consisting of all permutations of four binary variables were compared under proton radiation. Namely, the four variables were if the L2 Cache was on or off, whether the system was performing matrix multiplication (MM) or sitting idle, whether there was a large number of drivers installed or the bare minimum, and whether those drivers were loaded into the kernel or not. The test setup can be seen in Fig. 3.

The L2 Cache variable gives us insight into how the memory hierarchy affects reliability. It is common to disable any higher-level caches in a space platform to increase the reliability, though with a significant cost of performance. Similarly, the use of matrix multiplication as an application allows the data to constantly be moved around in memory, which can affect which bits can be critical to the kernel and to the application. Drivers are typically required for various hardware interfaces. However, drivers require access to kernel space in memory which can lead them to kernel panics if they crash. Therefore, testing how the number of drivers installed, and how many are loaded into memory should give an understanding for how the driver's existence in kernel space can affect the reliability. Fig. 3 shows the test setup.

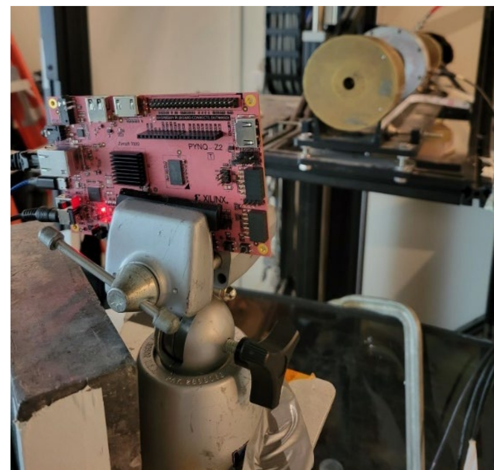

Fig. 3. Test setup picture.

The results of the tests were separated into configurations where the L2 cache was on and off, shown in Figs. 4 and 5, respectively. When the L2 cache is ON, the cross section is significantly worse for the IDLE configurations compared to the MM configurations. This is most likely due to the critical data retrieval processes of the DUT. When matrix multiplication is processing, critical kernel data is being flushed out of the cache to make room for the matrix data. If the system is idling, then that critical data never gets flushed out of the cache and thus has a higher chance of corruption, especially since the DDR3 SDRAM chip was not under irradiation. Additionally, the UNLOADED configurations were significantly better than the LOADED configurations. This implies that the drivers being loaded and active in the kernel do affect the reliability of the system. This is expected since the drivers have memory access to kernel space, even when they aren't actively being used. However, the number of drivers installed and loaded do not seem to have a significant effect on cross section. We surmise that this could be because there wasn't enough of a significant difference in the number of drivers between the configurations, or because the drivers were not being actively used on real hardware devices. In the L2 cache OFF configuration, any patterns are much more difficult to discern, most likely due to there being not enough memory just in the L1 cache to hold critical data. Further data and statistical analysis are needed to gather any conclusions of the L2 cache OFF configurations [16].

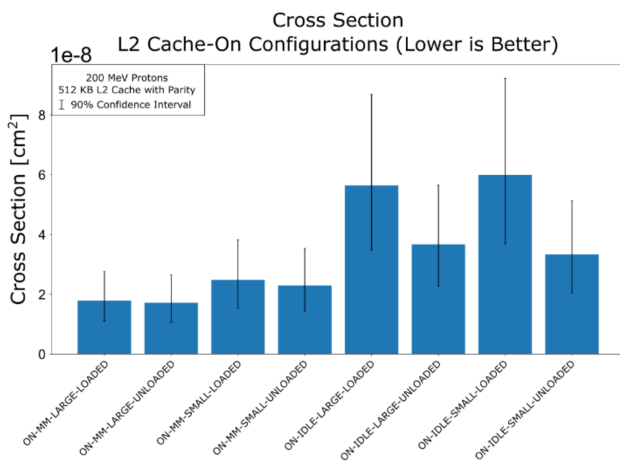

Fig. 4. Results with L2 Cache On.

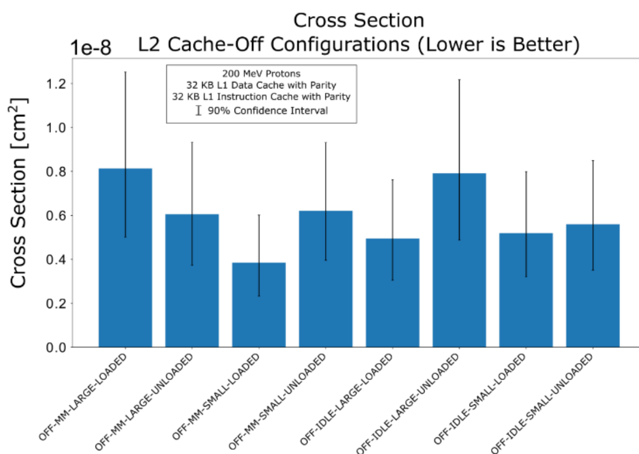

Fig. 5. Results with L2 Cache Off

V. SUMMARY

We have presented data from recent radiation tests on a variety of devices including several commercial parts. It is the authors' recommendation that this data be used cautiously as many tests were conducted under application- or lot-specific test conditions. We also highly recommend that lot-specific testing be performed on any suspect or commercial device.

VI. ACKNOWLEDGMENT

The authors would like to acknowledge the sponsors of this effort: NASA Electronic Parts and Packaging Program (NEPP) and NASA Flight Projects. The authors thank members of the Radiation Effects and Analysis Group (REAG) who contributed to the test results presented here; Edward J. Wyrwas, Rebekah A. Austin, Stephen K. Brown, Martin A. Carts, Yevgeniy Gerashchenko, James Forney, Hak Kim, Kenneth LaBel, Ray Ladbury, Kenny O'Connor, Anthony Phan, Scott Stansberry, Craig Stauffer, Carl Szabo, and members of the NASA GSFC Parts, Packaging, & Assembly Technologies Branch: Dillon Johnstone, and Carson Goettlicher.

VII. REFERENCES

1. Kenneth A. LaBel, Lewis M. Cohn, and Ray Ladbury, "Are Current SEE Test Procedures Adequate for Modern Devices and Electronics Technologies?," http://radhome.gsfc. nasa.gov/radhome/papers/HEART08_LaBel.pdf.
2. JEDEC Government Liaison Committee, Test Procedure for the Management of Single-Event Effects in Semiconductor Devices from Heavy Ion Irradiation," JESD57A, https://www.jedec.org/standards-documents/docs/jesd-57, Nov. 2017.
3. NI LabVIEW System Design Software, http://www.ni.com/labview/
4. NASA/GSFC Radiation Effects and Analysis home page, http://radhome.gsfc.nasa.gov.
5. NASA Electronic Parts and Packaging Program home page, http://nepp.nasa.gov.
6. Department of Defense "Test Method Standard Microcircuits," MIL-STD-883 Test Method 1019.9 Ionizing radiation (total dose) test procedure, June 7, 2013, https://landandmaritimeapps.dla.mil/Downloads/MilSpec/Docs/MIL-STD-883/std883.pdf.
7. B. Hyman, "Texas A&M University Cyclotron Institute, K500 Superconducting Cyclotron Facility," http://cyclotron.tamu.edu/facilities.htm, Jul. 2003.
8. Michael B. Johnson, Berkeley Lawrence Berkeley National Laboratory (LBNL), 88-Inch Cyclotron Accelerator, Accelerator Space Effects (BASE) Facility http://cyclotron.lbl.gov.
9. Michigan State University's Facility for Rare Isotope Beams (FRIB) heavy-ion accelerator, https://frib.msu.edu/science/fsee.
10. Brookhaven National Laboratory's NASA Space Radiation Laboratory (NSRL), https://www.bnl.gov/nsrl/.
11. NASA Goddard Space Flight Center Radiation Effects Facility https://radhome.gsfc.nasa.gov/radhome/ref/GSFC_ REF.html.
12. C. M. Castaneda, University of California at Davis (UCD) "Crocker Nuclear Laboratory (CNL) Radiation Effects Measurement and Test Facility," IEEE NSREC01 Data Workshop, pp. 77-81, Jul. 2001.
13. Massachusetts General Hospital (MGH) Francis H. Burr Proton Therapy, https://www.massgeneral.org/cancer-center/radiation-oncology/treatments-and-services/proton-therapy.

14. Edward P. Wilcox, "Single-Event Effects Test Report Micron MTFDHBK256TDP-1AT12AIYY NVMe Solid-State Drive," NASA Technical Memorandum (TM) test report, Jan. 2024. [Online] Available: https://nepp.nasa.gov/docs/ tasks/040-Microelectronics-Nonvolatile-Memory/NEPP-NASA-TM-23-009-MTFDHBK256TDP-2024Jan-20240001937.pdf.
15. Edward P. Wilcox, Adia Wood, Gregory Allen, Martin Carts, Megan Casey, “Solid State Drive Radiation Assurance With Active Testing,” late news submission to be published in the IEEE Trans. on Nucl. Sci., Dec. 2024.
16. Seth Roffe, "Single-Event Effects Test Report Linux Operating System Configurations on TUL PYNQ-Z2 Software," NASA Technical Memorandum (TM) test report, Aug. 2023. [Online] Available: https://nepp.nasa.gov/docs/tasks/065-GPU-Devices/NEPP-NASA-TM-20-004-Xilinx-ZYNQ-XC7Z020-1CLG400C-SEE-Test-Report-MGH-2023Aug.pdf.
17. Seth Roffe, Scott Stansberry, Jeffrey Grosman, Jeffry Milrod, Manish Sinha, Uzzal Podder, “EdgeCortix SAKURA-I Machine-Learning, PCIe Accelerator SEE Proton Test,” NASA Technical Memorandum (TM) test report, Jan. 2024. [Online] Available: https://nepp.nasa.gov/docs/tasks/075-EEE-Parts-Assurance/NEPP-NASA-TM-24-001-EdgeCortix-SAKURA-I-2024Jan-Proton-Test-Report-20240006221.pdf.
18. Landen D. Ryder, Jason M. Osheroff, Megan C. Casey, Matthew B. Joplin, "Single Event Effect Testing of the SSDI SFF6661 N-Channel Power MOSFET," NASA Technical Memorandum (TM) test report, , Apr. 2023. [Online] Available: https://radhome.gsfc.nasa.gov/radhome/papers/2023-Ryder-Landen-NASA-TM-23-003-SSDI-SFF6661-2023Apr-SEE-Test-Report-20230017327.pdf.
19. Jean-Marie Lauenstein, Dillon Johnstone, Carson Goettlicher, Jonathan Barth, “Proton Radiation Test Report for the Opto Diode OD-110L 850 nm LED,” NASA Technical Memorandum (TM) test report, Aug 2023. [Online] Available: https://radhome.gsfc.nasa.gov/radhome/papers/2023-Lauenstein-NASA-TM-23-028-OD-110L-2023Aug-Test-Report-20240002481.pdf.